Photocatalysis
https://www.sciltp.com/journals/photocatalysis

Article

Efficient Light Initiated One-Pot Synthesis of Benzimidazoles over PtS/$ZnIn_2S_4$ Promoted by RGO

Jiaqi Wang [1,2], Tianyi Liu [1], Xiao Du [1] and Zhaohui Li [1,*]

[1] Research Institute of Photocatalysis, State Key Laboratory of Photocatalysis on Energy and Environment, College of Chemistry, Fuzhou University, Fuzhou 350116, China
[2] Fujian Province Colleges and University Engineering Research Center of Solid Waste Resource Utilization, College of Chemistry and Materials Science, Longyan University, Longyan 364012, China
* Correspondence: zhaohuili@fzu.edu.cn; Tel./Fax: +86-591-22865855

How To Cite: Wang, J.; Liu, T.; Du, X.; et al. Efficient Light Initiated One-Pot Synthesis of Benzimidazoles over PtS/$ZnIn_2S_4$ Promoted by RGO. *Photocatalysis* **2025**, *1*(1), 5. https://doi.org/10.53941/photocatalysis.2025.100005

Received: 8 September 2025
Revised: 10 November 2025
Accepted: 18 November 2025
Published: 19 November 2025

Abstract: PtS/RGO/$ZnIn_2S_4$ nanocomposites, fabricated via a rapid microwave-assisted process followed by photoreduction, were found to be an efficient multifunctional catalyst for the visible-light-driven one-pot synthesis of benzimidazoles from *o*-phenylenediamines and alcohols. By modulating the composition of the photocatalytic system to affect its adsorption toward the substrates and the intermediates, an optimum performance with 91.4% of 2-phenylbenzimidazole was obtained over irradiated 2.0 wt% PtS/1.0 wt% RGO/$ZnIn_2S_4$. It was revealed that the superior performance over 2.0 wt% PtS/1.0 wt% RGO/$ZnIn_2S_4$ arises from RGO, which enhances the adsorption toward benzaldehyde, the intermediate, as well as from the PtS, which promotes both alcohol dehydrogenation and intermediates condensation, to enable an efficient one-pot benzimidazole synthesis under visible light. This study reveals that in addition to the required different catalytic sites required, an efficient one-pot tandem/cascade reaction also necessitates to regulate the reaction rate of the individual reaction step, accomplished through tuning of the composition of the catalyst. This work also highlights the considerable potential of metal sulfide-based multifunctional catalysts for light-initiated one-pot tandem/cascade reactions.

Keywords: one-pot tandem/cascade reaction; benzimidazoles; PtS/RGO/$ZnIn_2S_4$ nanocomposites; visible light

1. Introduction

Utilizing visible light to trigger organic syntheses is a sustainable and green strategy for value-added chemicals production [1]. Especially, light-initiated one-pot tandem/cascade reactions, enabling multi-step transformations without intermediate isolation, is highly attractive [2]. The mild reaction strategy enhances energy efficiency and minimizes thermally derived side products production, significantly simplifying the reaction mixture [3–7]. Consequently, one-pot tandem/cascade reactions initiated by visible light have attracted significant attention as a promising avenue toward sustainable chemical production.

Benzimidazole, as an important class of heterocyclic compounds, have gained considerable interest owing to its diverse applications as bioactive molecules and therapeutic agents [8]. Although traditional method for benzimidazoles production involves the condensation of *o*-phenylenediamines with carboxylic acids or their derivatives, it requires harsh acidic conditions and high temperature (>200 °C), and sometimes stoichiometric strong oxidants are also needed [9,10]. The photo-initiated direct coupling of *o*-phenylenediamines with readily accessible alcohols is an environmentally safe and atom-economical approach through a one-pot tandem dehydrogenation/condensation, and is generally believed to follow three consecutive steps, i.e., (i)

dehydrogenative conversion of alcohols to aldehydes, (ii) condensation of *o*-phenylenediamine with the resultant aldehydes to afford benzimidazolines as the intermediates, and (iii) subsequent dehydrogenation to generate benzimidazoles (Scheme 1) [11,12]. The realization of such a light-initiated one-pot tandem/cascade process generally necessitates a multifunctional catalyst that integrates high intrinsic photocatalytic activity, catalytic sites for H_2 evolution, and Lewis acidic/basic sites to facilitate condensation [13]. Besides the necessary diversity of catalytic sites, precise matching of all constituent reaction steps is also essential to ensure overall cascade/tandem efficiency, which can be accomplished either through the modulation of reaction conditions or by adjusting the composition of the catalyst [7]. As compared with the regulation of the reaction medium, which has already been demonstrated for optimizing individual reaction steps over Pt/Ni-Fe-MOF nanosheets in our previous work [14], the development of multifunctional photocatalyst by modulating its composition for this reaction remains largely unexplored.

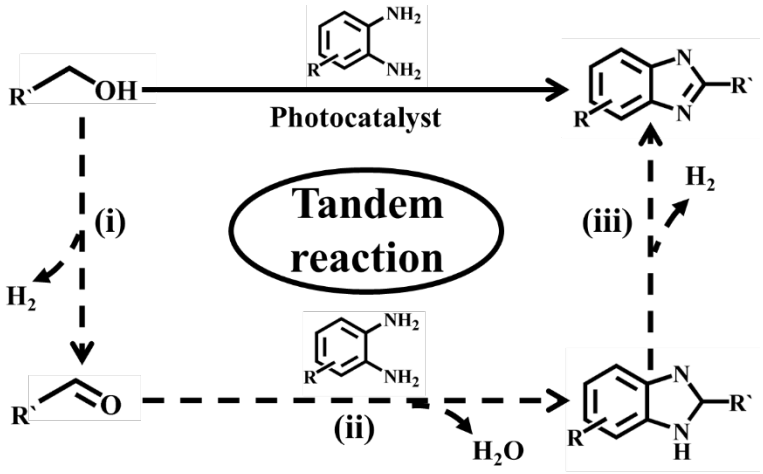

Scheme 1. Schematic illustration of the reaction pathway in the light initiated one-pot synthesis of benzimidazoles from *o*-phenylenediamines and alcohols.

Ascribable to their visible-light absorption and moderate oxidation potential of the photogenerated holes, hexagonal $ZnIn_2S_4$ as a ternary chalcogenide is considered as an attractive candidate for photocatalytic organic reaction [15–18]. Given the critical role of intermediate adsorption in enabling the tandem photocatalytic production of benzimidazoles from alcohols and *o*-phenylenediamines, owing to its planar polycyclic aromatic hydrocarbon structure, reduced graphene oxide (RGO) emerges as a promising functional component in facilitating the adsorption toward aldehyde, the intermediate, via π-π stacking interactions [19]. Furthermore, co-catalysts like PtS nanoparticles are essential to provide both Lewis acidic/basic sites for condensation/cyclization of the intermediates as well as hydrogen evolution capability [7]. Therefore, a rationally designed PtS/RGO/$ZnIn_2S_4$ nanocomposite is proposed as an effective catalytic system for photocatalytic production of benzimidazoles from alcohols and *o*-phenylenediamines.

In this manuscript, we reported a rapid microwave-assisted process coupled with subsequent photoreduction for PtS/RGO/$ZnIn_2S_4$ preparation. The resultant PtS/RGO/$ZnIn_2S_4$ was applied as a multifunctional photocatalyst in the one-pot reaction of alcohols and *o*-phenylenediamines to form benzimidazoles. A superior performance was observed by modulating the composition of the photocatalytic system to affect its adsorption toward the substrates and the intermediates. This work highlights that beyond the catalytic active sites, modulating individual reaction steps by tuning of the composition of the catalyst is critical for achieving an efficient overall process, which is an aspect largely overlooked in prior research.

2. Experimental Section

2.1. Preparations

Graphene oxide (GO) was obtained from a modified Hummers method [20]. To prepare reduced GO (RGO)/$ZnIn_2S_4$ nanocomposites, varying quantities of GO were first ultrasonically dispersed for 40 min in a binary solvent system consisting of ethylene glycol (EG) and *N*,*N*-dimethylformamide (DMF) (60 mL, 1:1/*v*:*v*). Then $ZnCl_2$ (0.136 g, 1.0 mmol), $InCl_3 \cdot 4H_2O$ (0.586 g, 2.0 mmol), and thioacetamide (TAA) (0.300 g, 4.0 mmol) were introduced into the aforementioned suspension under continuous stirring. The resulting suspension was transferred to a sealed Teflon-lined autoclave and subjected to microwave-assisted heating (Ethos A, Milestone, Italy) at 180 °C for 90 min.

After reaction, the resultant product was collected by centrifugation, washed with deionized (DI) water and ethanol, and dried at 60 °C. The RGO/$ZnIn_2S_4$ nanocomposites with different RGO loadings were designated as x wt% RGO/$ZnIn_2S_4$ (x is the weight ratio of RGO:$ZnIn_2S_4$, x = 1.0 and 2.0).

PtS/RGO/$ZnIn_2S_4$ were fabricated through a photoreduction method. Typically, RGO/$ZnIn_2S_4$ (0.2 g) in a Schlenk tube was degassed and purged with N_2. Different amounts of H_2PtCl_6 in CH_3OH (10 mL) was injected into the above Schlenk tube before the dissolved O_2 was removed. The suspension was then irradiated with Xe lamp (PLS-SXE300c, Beijing Perfect light, 300 W) for 180 min. After irradiation, the obtained catalyst was dried at 60 °C before thoroughly washed with ethanol.

For comparison, $ZnIn_2S_4$ was prepared similarly without GO. 2.0 wt% PtS/$ZnIn_2S_4$ nanocomposite was prepared by photoreduction of H_2PtCl_6 on bare $ZnIn_2S_4$ using CH_3OH as a sacrificial agent.

2.2. Catalytic Reactions

The photocatalytic reactions were conducted in a sealed Schlenk tube irradiated with a 3 W blue LED lamp (GeAoLEDs, H106064). In a typical procedure, *o*-Phenylenediamine (5.4 mg, 50 μmol) in benzyl alcohol (3 mL) saturated with N_2 was added to a Schlenk tube containing 20 mg of catalyst. The reaction system was illuminated with blue LED lamp for 20 h. At the end of reaction, the sample was filtered with a 0.22 μm porous membrane and the filtrate was analyzed by GC-FID and GC-MS, while the gaseous products were measured with GC-TCD.

The adsorption of 2.0 wt% PtS/1.0 wt% RGO/$ZnIn_2S_4$ and $ZnIn_2S_4$ toward the benzaldehyde were performed in dark under N_2 atmosphere for 20 h, with continuous stirring.

The detail of the Characterizations is provided in the Supplementary Materials.

3. Results and Discussion

RGO/$ZnIn_2S_4$ nanocomposites with varying amount of GO were obtained by a rapid microwave-assisted method. The XRD pattern of the resultant catalyst (take 1.0 wt% RGO/$ZnIn_2S_4$ for example) depicts diffraction peaks at 21.6°, 27.6°, 30.4° and 47.2°, assignable to (006), (102), (104) and (110) planes of hexagonal $ZnIn_2S_4$ (JCPDS-03-065-2023) [21], confirming that the incorporation of RGO does not alter the $ZnIn_2S_4$ structure (Figure 1). Although the XRD patterns show no characteristic peaks for either GO or RGO, the presence of RGO in the nanocomposite was evidenced by Raman spectra through its characteristic D/G bands at 1345 cm^{-1} and 1596 cm^{-1} [22] (Figure S1). XPS analysis also confirms the formation of RGO as evidenced from a dramatically decreased C–O intensity at 286.40 eV compared to that of original GO (Figure S2). To obtain PtS/RGO/$ZnIn_2S_4$ nanocomposites, the as-obtained RGO/$ZnIn_2S_4$ were treated with $[PtCl_6]^{2-}$ in CH_3OH under visible light. The $[PtCl_6]^{2-}$ reduction was verified by the change of the suspension color from dark green to brown under visible light and was subsequently confirmed by the Pt 4f XPS spectrum of PtS/RGO/$ZnIn_2S_4$, which exhibits two peaks at 75.81 eV and 72.46 eV, ascribable to Pt^{2+} in the Pt $4f_{5/2}$ and Pt $4f_{7/2}$ regions, respectively (Figure 2a). Furthermore, as compared to that in RGO/$ZnIn_2S_4$ (Figure S3), it is obvious that the S 2p XPS spectrum of 2.0 wt% PtS/1.0 wt% RGO/$ZnIn_2S_4$ should be fitted into two sets of peaks, where the peaks at 162.57 eV and 161.39 eV can be assigned to S $2p_{1/2}$ and S $2p_{3/2}$ in PtS, and the other at 163.05 eV and 161.87 eV corresponding to S $2p_{1/2}$ and S $2p_{3/2}$ in $ZnIn_2S_4$ (Figure 2b), confirming the successful photoreduction of $[PtCl_6]^{2-}$ to form PtS deposited over RGO/$ZnIn_2S_4$ (with its XPS spectra in C 1s, Zn 2p, In 3d regions also shown in Figure S4). The TEM image displays a morphology of flower-like microspheres assembled from numerous interwoven ultrathin nanosheets in the 2.0 wt% PtS/1.0 wt% RGO/$ZnIn_2S_4$ (Figures 3a). The distinct lattice fringes of 0.302 nm and 0.324 nm were attribute to (101) plane of PtS and (102) plane of hexagonal $ZnIn_2S_4$ [13,23] in HRTEM image (inset in Figure 3b). Moreover, lattice fringes corresponding to hexagonal $ZnIn_2S_4$ and PtS are interwoven with amorphous regions of RGO, confirming intimate contact among hexagonal $ZnIn_2S_4$, PtS and RGO nanosheets (Figure 3b). Element mapping further confirms the uniform distribution of Pt, C, Zn, In and S (Figure 3c). The amount of Pt in 2.0 wt% PtS/1.0 wt% RGO/$ZnIn_2S_4$ nanocomposite was quantified as ~1.88 wt% by ICP-OES, which closely corresponds to the quantity of Pt incorporated.

The UV-vis DRS spectrum of the 2.0 wt% PtS/1.0 wt% RGO/$ZnIn_2S_4$ is presented in Figure 4. Compared to the spectra of bare $ZnIn_2S_4$ and 1.0 wt% RGO/$ZnIn_2S_4$, the ternary 2.0 wt% PtS/1.0 wt% RGO/$ZnIn_2S_4$ shows significant enhancement in absorption within the 420–800 nm range, consistent with the color change of the 2.0 wt% PtS/1.0 wt% RGO/$ZnIn_2S_4$ nanocomposites from dark green to brown after the introduction of PtS into RGO/$ZnIn_2S_4$ nanocomposites.

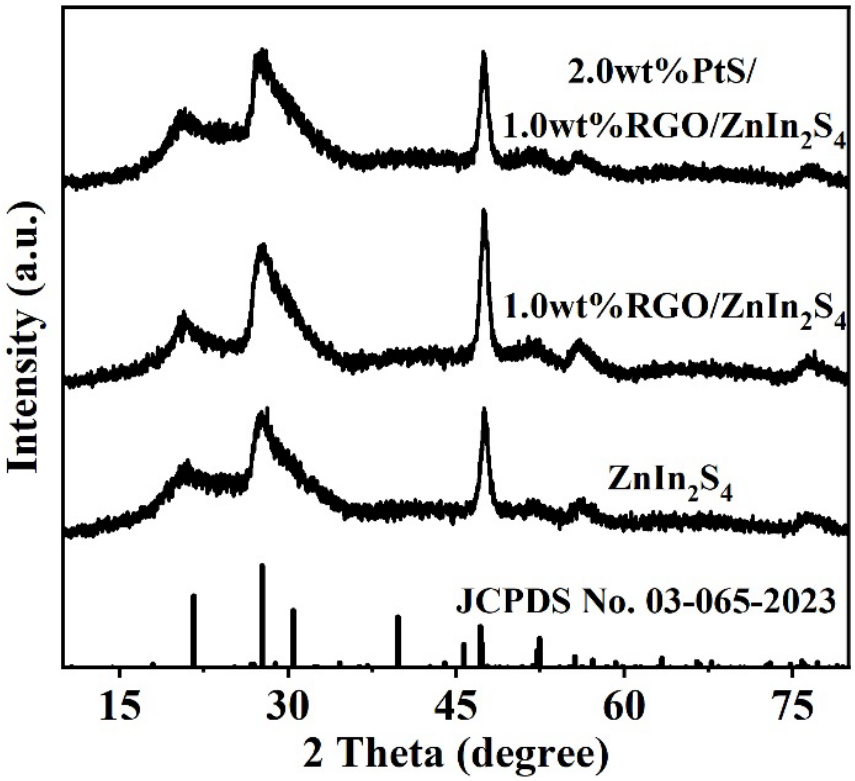

Figure 1. XRD patterns of 2.0 wt% PtS/1.0 wt% RGO/$ZnIn_2S_4$, 1.0 wt% RGO/$ZnIn_2S_4$ and $ZnIn_2S_4$.

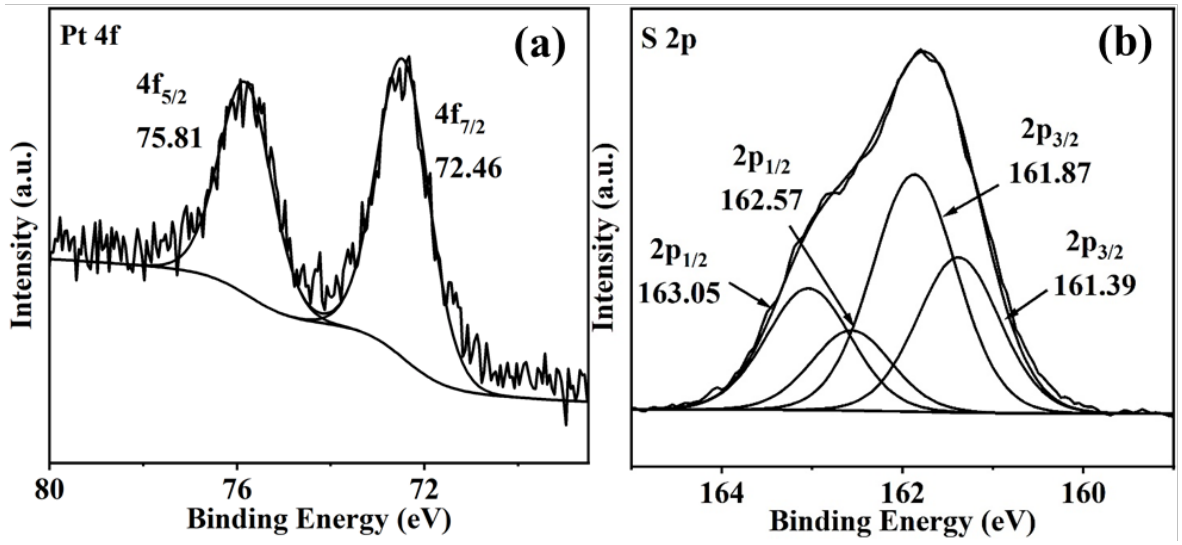

Figure 2. XPS spectra of (**a**) Pt 4f and (**b**) S 2p in 2.0 wt% PtS/1.0 wt% RGO/$ZnIn_2S_4$ nanocomposite.

The performance of the synthesized PtS/RGO/$ZnIn_2S_4$ nanocomposite was evaluated for the one-pot production of benzimidazoles from *o*-phenylenediamine (1a) and alcohols under visible light, and 2.0 wt% PtS/1.0 wt% RGO/$ZnIn_2S_4$ in benzyl alcohol (2a), serving both as the solvent and the reactant, was initially used in the reaction. 98.8% of 1a was transformed after 20 h irradiation, with a yield of 91.4% to the target product 2-phenylbenzimidazole (3a), together with minor 2,3-dihydro-2-phenyl-1H-benzimidazole (3b) as the byproducts (2.1%), which was detected and verified in GC and GC-MS with its *m*/*z* at 196 (Figures S5 and S6e). Benzaldehyde (197.5 μmol) and quantitative H_2 (250.7 μmol) were also obtained (Table 1, entry 1). No product was detected when the reaction was performed in absence of either light or 2.0 wt% PtS/1.0 wt% RGO/$ZnIn_2S_4$ (Table 1, entries 2, 3). Bare $ZnIn_2S_4$, 1.0 wt% RGO/$ZnIn_2S_4$ as well as 2.0 wt% PtS/$ZnIn_2S_4$ all showed inferior activities as compared to that of 2.0 wt% PtS/1.0 wt% RGO/$ZnIn_2S_4$, with only 3.5%, 6.2% and 74.4% to 3a generated under otherwise similar conditions (Table 1, entries 4–6). These indicated that the one-pot 3a production from 1a and 2a is truly induced over irradiated $ZnIn_2S_4$, while both RGO and PtS play promoting effects for this reaction.

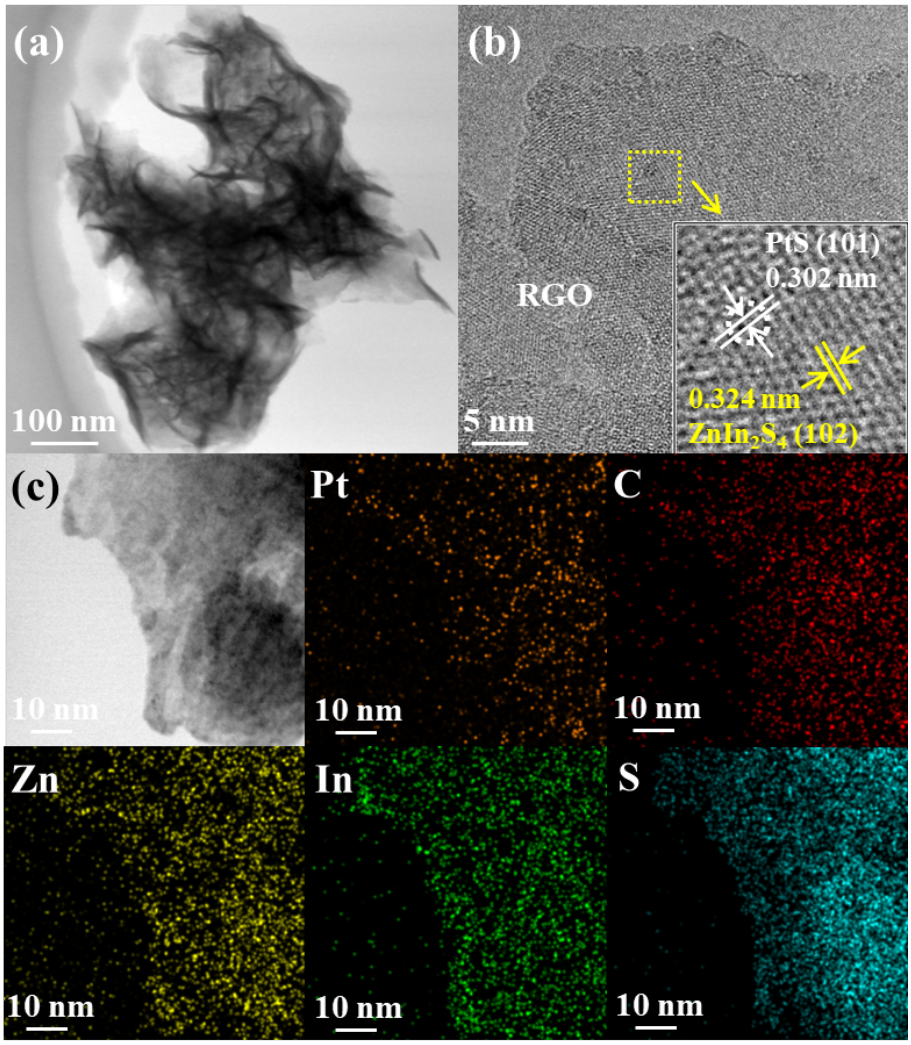

Figure 3. (**a**) TEM, (**b**) HRTEM and (**c**) mapping images of 2.0 wt% PtS/1.0 wt% RGO/$ZnIn_2S_4$ nanocomposite.

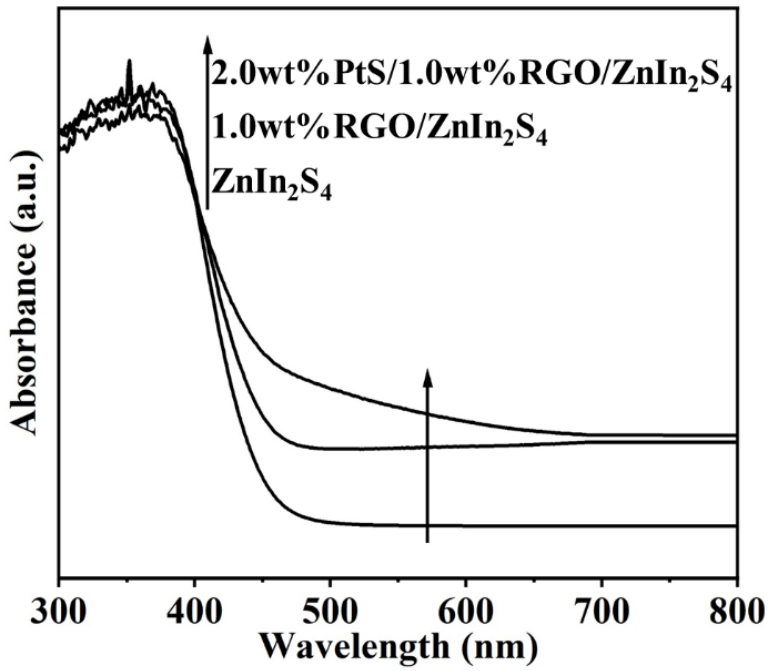

Figure 4. UV-vis DRS spectra of 2.0 wt% PtS/1.0 wt% RGO/$ZnIn_2S_4$, 1.0 wt% RGO/$ZnIn_2S_4$ and $ZnIn_2S_4$.

Table 1. Light initiated one-pot synthesis of 2-phenylbenzimidazole from *o*-phenylenediamine and benzyl alcohol under different conditions.

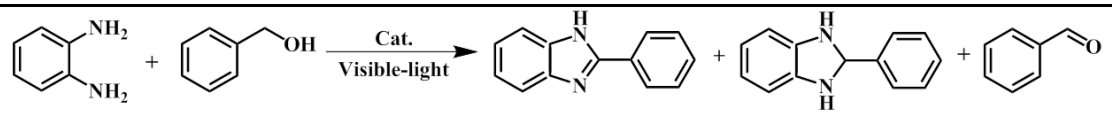

1a **2a** **3a** **3b** **3c**

Entry	Cat.	H_2 /μmol	Conv. /%	Yield/%		Benzaldehyde (3c)/μmol
				3a	3b	
1	2.0 wt% PtS/1.0 wt% RGO/$ZnIn_2S_4$	250.7	98.8	91.4	2.1	197.5
2 [a]	2.0 wt% PtS/1.0 wt% RGO/$ZnIn_2S_4$	/	/	/	/	/
3 [b]	/	/	/	/	/	/
4	$ZnIn_2S_4$	457.8	97.3	3.5	2.0	178.9
5	1.0 wt% RGO/$ZnIn_2S_4$	527.7	98.0	6.2	2.3	120.7
6	2.0 wt% PtS/$ZnIn_2S_4$	242.1	97.6	74.4	2.2	183.5
7	2.0 wt% PtS/2.0 wt% RGO/$ZnIn_2S_4$	310.5	99.1	63.7	2.1	295.5

Reaction conditions: Cat.: 20 mg; *o*-phenylenediamine: 1a, 50 μmol; benzyl alcohol: 2a, 3 mL; N_2; blue light; reaction time: 20 h. [a] Without light; [b] No catalyst.

The time-dependent transformation of benzyl alcohol and *o*-phenylenediamine were also monitored over 2.0 wt% PtS/1.0 wt% RGO/$ZnIn_2S_4$ (Figure 5). It was observed that the amount of *o*-phenylenediamine gradually decreased, achieving complete conversion within 20 h. Meanwhile, the yield of the desirable 2-phenylbenzimidazole increased steadily over irradiation time. In contrast, although the amount of benzaldehyde increased throughout the entire irradiation period, a rapid increase was only observed after 8 h. Obviously, in the first 8 h, a portion of the aldehyde produced via alcohol dehydrogenation rapidly condenses with *o*-phenylenediamine to form 2,3-dihydro-2-phenyl-1H-benzimidazole, the intermediate (Scheme 1, step ii). The observation that 2,3-dihydro-2-phenyl-1H-benzimidazole remains at a relatively low concentration throughout the reaction period implies that the dehydrogenation of 2,3-dihydro-2-phenyl-1H-benzimidazole to form the target 2-phenylbenzimidazole is fast. Therefore, similar to prior reports, the one-pot production of benzimidazole from alcohol and *o*-phenylenediamine over PtS/RGO/$ZnIn_2S_4$ nanocomposite also undergoes several successive steps. As depicted in Figure 6, the reaction is initiated by the photogenerated electrons and holes over irradiated $ZnIn_2S_4$. Owing to the lower PtS work function (ca. 4.29 eV) relative to the $ZnIn_2S_4$ conduction band (−0.97 V vs. NHE) [24], the photogenerated electrons can thermodynamically migrate from excited $ZnIn_2S_4$ to PtS in PtS/RGO/$ZnIn_2S_4$, which act as a cocatalyst to promote the dehydrogenation reaction, while holes in $ZnIn_2S_4$ mediate the oxidization of adsorbed benzyl alcohol to form benzaldehyde with proton release. The Lewis acidic sites in PtS/RGO/$ZnIn_2S_4$ nanocomposite facilitate the condensation of the benzaldehyde formed in-situ and the *o*-phenylenediamine, yielding the Schiff base intermediate 2,3-dihydro-2-phenyl-1H-benzimidazole. This intermediate subsequently undergoes dehydrogenation to affords the targeted product 2-phenylbenzimidazole, with concomitant H_2 generation. Since PtS acts both as a cocatalyst for photocatalytic dehydrogenation of benzyl alcohol and the Lewis acidic site for condensation, the absence of PtS would significantly suppress the performance of photocatalytic one-pot production of 2-phenylbenzimidazole from benzyl alcohol and *o*-phenylenediamine. As observed in the reaction over bare $ZnIn_2S_4$, although an exceptionally high conversion of 1a (97.3%) was achieved, only 3.5% of 3a was obtained (Table 1, entry 4). In addition, the color changed from the original light yellow to dark brown, implying the formation of poly-phenylenediamine byproduct since *o*-phenylenediamine is susceptible to polymerize under light irradiation [25]. It is proposed that the introduction of RGO into $ZnIn_2S_4$ enhances the adsorption toward benzaldehyde, the intermediate, while the introduction of PtS into $ZnIn_2S_4$ overcomes the inefficient condensation between benzaldehyde and 1a, and inhibits the polymerization of 1a. As a result, the co-deposition of PtS and RGO on $ZnIn_2S_4$ promotes the efficient one-pot reaction of phenylenediamines and alcohols to form benzimidazoles under visible light. This assumption is supported by the detection of less amount of benzaldehyde (120.7 μmol) observed in a reaction system of 1.0 wt% RGO/$ZnIn_2S_4$ than that of $ZnIn_2S_4$ (178.9 μmol) (Table 1, entries 4, 5), as well as the result from the adsorption experiment by showing higher adsorption capacity towards benzaldehyde after the introduction of RGO into $ZnIn_2S_4$ (11.4 μmol) as compared to that of bare $ZnIn_2S_4$ (3.25 μmol), which is supposed to be ascribed to the existence of the planar polycyclic aromatic hydrocarbon structure in RGO [26]. These results clearly indicated that the introduced RGO can

greatly enhance the adsorption toward the intermediate in the catalytic system, which is supposed to promote the condensation between alcohols and *o*-phenylenediamines. That is to say, by influencing the adsorption of benzaldehyde intermediate on catalyst, as well as promoting the dehydrogenation of alcohol and the condensation intermediates, an efficient overall tandem/cascade reaction is possible to be realized by modulating the rate of the individual reaction step. To exclude the influence of the specific surface area on the activity, the specific surface area of 2.0 wt% PtS/1.0 wt% RGO/$ZnIn_2S_4$, 1.0 wt% RGO/$ZnIn_2S_4$ and $ZnIn_2S_4$ have also been measured (Figure S7). The specific surface area of 2.0 wt% PtS/1.0 wt% RGO/$ZnIn_2S_4$ nanocomposite was 74.2 $m^2 \cdot g^{-1}$, comparable to that of 1.0 wt% RGO/$ZnIn_2S_4$ (80.3 $m^2 \cdot g^{-1}$) but lower than that of $ZnIn_2S_4$ (101.6 $m^2 \cdot g^{-1}$). This indicated that the superior photocatalytic activity observed over 2.0 wt% PtS/1.0 wt% RGO/$ZnIn_2S_4$ as compared with that of 1.0 wt% RGO/$ZnIn_2S_4$ or bare $ZnIn_2S_4$ cannot be ascribed to their specific surface area.

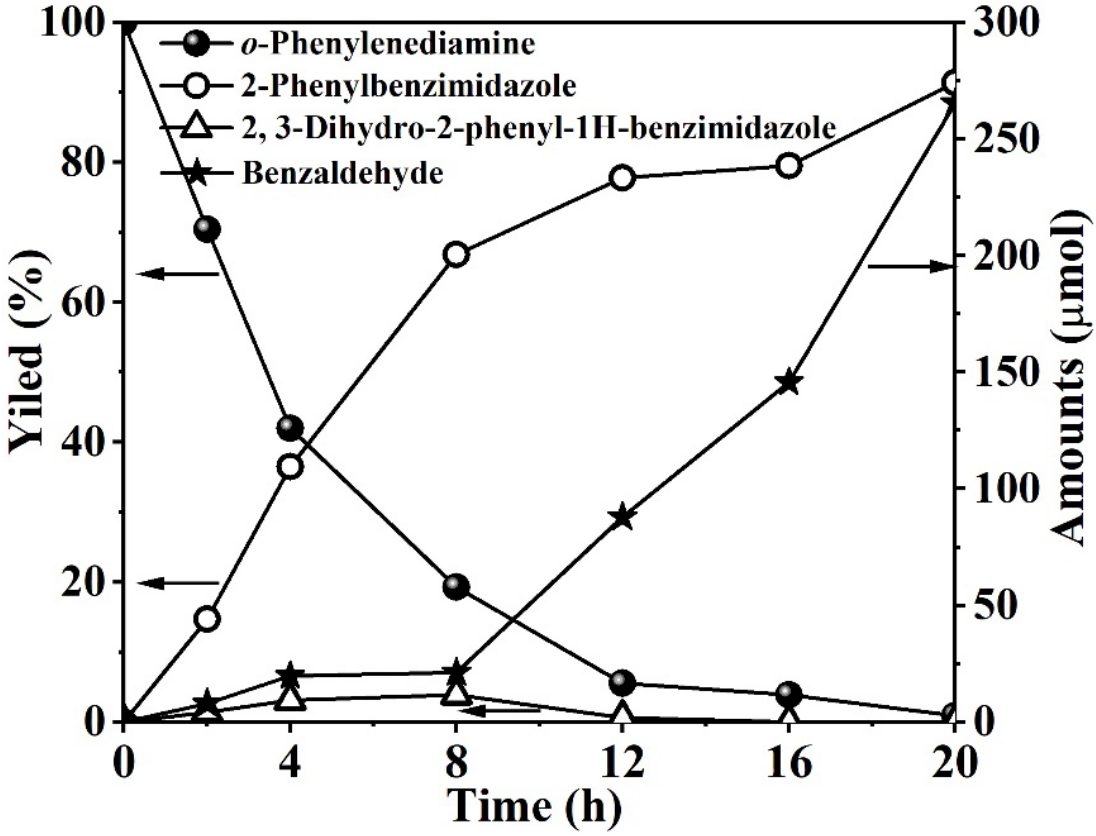

Figure 5. Time-dependent changes of the amounts of substrates and the products during the synthesis of 2-phenylbenzimidazole from *o*-phenylenediamine and benzyl alcohol over 2.0 wt% PtS/1.0 wt% RGO/$ZnIn_2S_4$ nanocomposite.

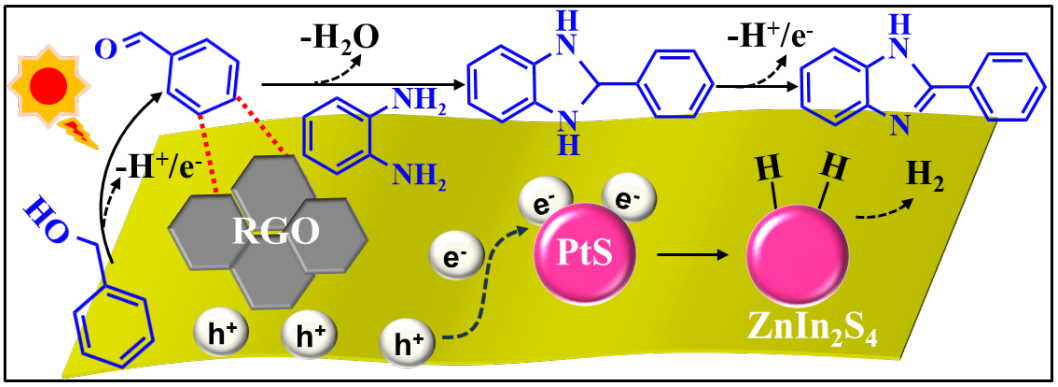

Figure 6. Proposed mechanism for the synthesis of benzimidazoles from *o*-phenylenediamines and alcohols over PtS/RGO/$ZnIn_2S_4$ nanocomposites under visible light.

Although RGO exhibits promoting effect for the adsorption toward benzaldehyde, an increasing of the RGO content from 1.0 to 2.0 wt% in PtS/RGO/$ZnIn_2S_4$ led to a decreased yield of 3a from 91.4% to 63.7% (Table 1,

entry 7). It is possible that overloading of RGO may cover the $ZnIn_2S_4$ surface and inhibit the photogenerated electrons' migration to PtS in PtS/RGO/$ZnIn_2S_4$.

The substrate scope of this photocatalytic system was successfully expanded to form various substituted benzimidazoles (Table 2, with the GC spectra and MS data of substituted benzimidazoles shown in Figures S8–S18). It was found that the *o*-phenylenediamines with electron-donating groups (–CH_3) afforded the corresponding benzimidazoles in good yields (63.8–70.0%). While those with electronic-withdrawing groups (–Cl and –Br) provided the yields ranging from 50.8% to 55.4%, slightly lower than that of *o*-phenylenediamines with electron-donating groups. Both methoxy or methyl-substituted benzyl alcohols reacted efficiently with *o*-phenylenediamines under visible-light irradiation, yielding products in 59.6–74.1%. Aliphatic alcohols (*n*-propanol and *n*-butanol) were also readily converted to the corresponding 2-substituted benzimidazoles in 58.3% to 60.8% yield. 2.0 wt% PtS/1.0 wt% RGO/$ZnIn_2S_4$ nanocomposite also exhibits high stability during the reaction, as evidenced from the cycling tests as well as its unchanged XRD pattern after the reaction (Figure 7).

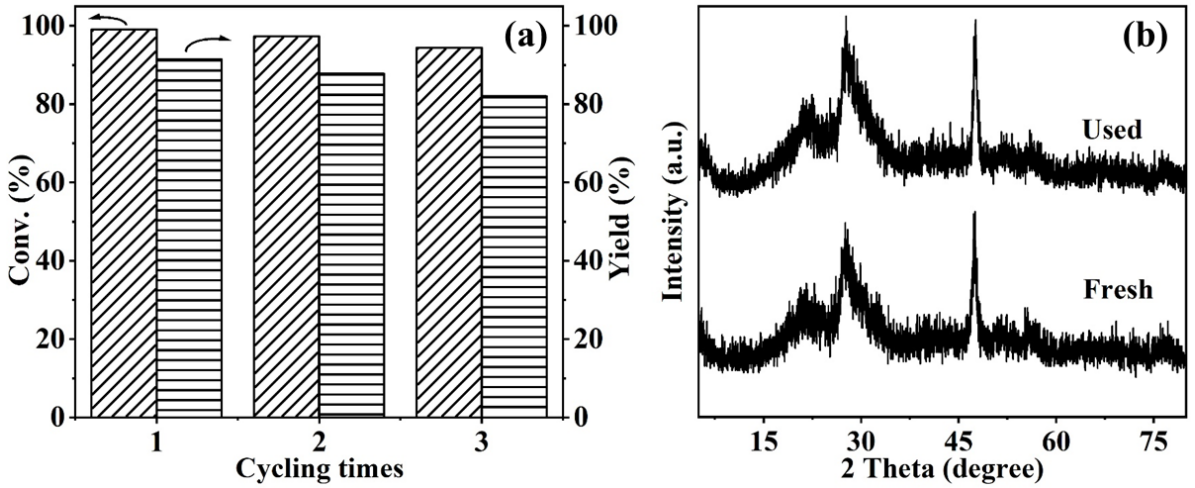

Figure 7. (**a**) Cycling tests for the light-initiated one-pot synthesis of 2-phenylbenzimidazole from *o*-phenylenediamine and benzyl alcohol over 2.0 wt% PtS/1.0 wt% RGO/$ZnIn_2S_4$; and (**b**) XRD patterns of fresh and used 2.0 wt% PtS/1.0 wt% RGO/$ZnIn_2S_4$.

Table 2. Light initiated one-pot synthesis of substituted benzimidazoles over 2.0 wt% PtS/1.0 wt% RGO/$ZnIn_2S_4$.

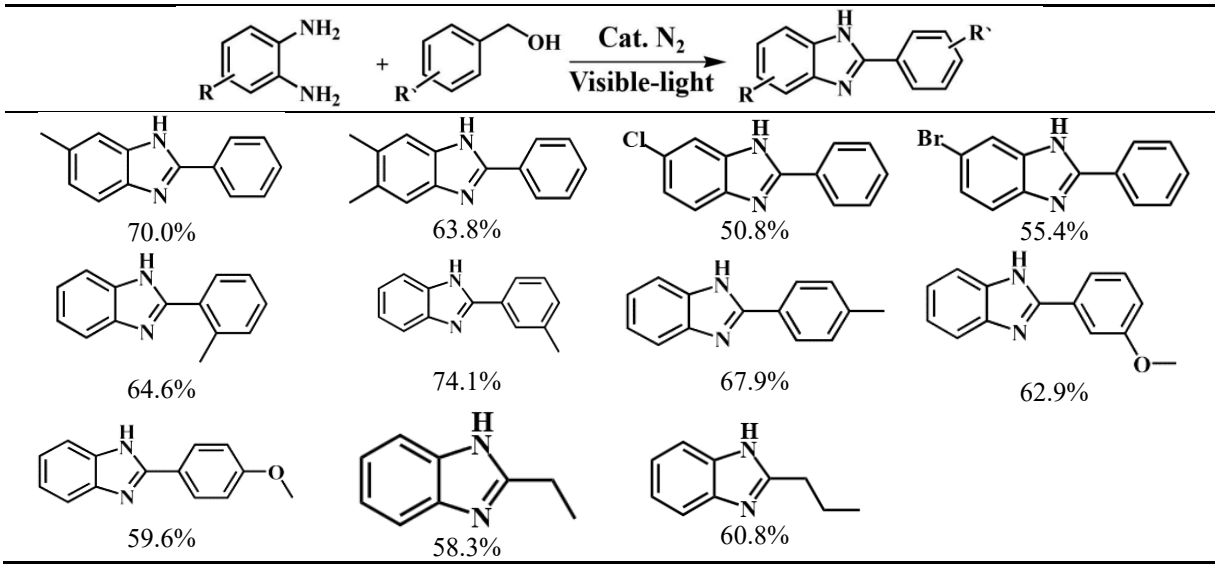

Reaction conditions: 2.0 wt% PtS/1.0 wt% RGO/$ZnIn_2S_4$: 20 mg; diamine: 50 μmol, alcohol: 3 mL; N_2; blue light; reaction time: 20 h.

4. Conclusions

PtS/RGO/$ZnIn_2S_4$ nanocomposites fabricated via a rapid microwave-assisted process serves as a highly efficient multifunctional catalyst for visible-light-driven one-pot benzimidazoles production from *o*-

phenylenediamines and alcohols. RGO in PtS/RGO/$ZnIn_2S_4$ nanocomposite enhances the adsorption toward the aldehyde, while PtS promotes the hydrogen evolution and the intermediates' condensation. The modulation of the nanocomposite's composition to affect its adsorption toward the substrates and the intermediates involved in the one-pot cascade/tandem reaction resulted in an optimum performance over 2.0 wt% PtS/1.0 wt% RGO/$ZnIn_2S_4$. This work indicated that, in addition to the required different catalytic sites, tuning the catalyst composition to regulate the reaction rates of individual steps is also key to achieving efficient one-pot tandem/cascade reactions. This finding also highlights the considerable promise of metal sulfide-based multifunctional catalysts for light-initiated one-pot tandem/cascade reactions.

Supplementary Materials

The additional data and information can be downloaded at: https://media.sciltp.com/articles/others/25111915 52157984/Photocatalysis-25090026-Supplementary-Materials-FC-done.pdf. Figure S1: Raman spectra of GO and 1.0 wt% RGO/$ZnIn_2S_4$ nanocomposites. Figure S2: XPS spectra of C1s in GO and 1.0 wt% RGO/$ZnIn_2S_4$. Figure S3: XPS spectrum of S 2p in 1.0 wt% RGO/$ZnIn_2S_4$. Figure S4: XPS spectra of (**a**) C1s, (**b**) Zn 2p, (**c**) In 3d in 2.0 wt% PtS/1.0 wt% RGO/$ZnIn_2S_4$. Figure S5: GC spectrum of the substrates and the products obtained from the synthesis of 2-phenylbenzimidazole from *o*-phenylenediamine and benzyl alcohol. Figure S6: Mass spectra of the substrates and the products obtained from the synthesis of 2-phenylbenzimidazole from *o*-phenylenediamine and benzyl alcohol (**a**: benzaldehyde; **b**: benzyl alcohol; **c**: o-phenylenediamine; **d**: 2-phenylbenzimidazole; **e**: 2,3-dihydro-2-phenyl-1H-benzimidazole). Figure S7: Nitrogen adsorption-desorption isotherms of 2.0 wt% PtS/1.0 wt% RGO/$ZnIn_2S_4$, 1.0 wt% RGO/$ZnIn_2S_4$ and $ZnIn_2S_4$. Figure S8: GC spectrum (**a**) and MS data (**b**) of the as-synthesized 6-methyl-2-phenyl-1H-benzoimidazole. Figure S9: GC spectrum (**a**) and MS data (**b**) of the as-synthesized 5,6-dimethyl-2-phenyl-1H-benzimidazole. Figure S10: GC spectrum (**a**) and MS data (**b**) of the as-synthesized 6-chloro-2-phenyl-1H-benzoimidazole. Figure S11: GC spectrum (**a**) and MS data (**b**) of the as-synthesized 6-bromo-2-phenyl-1H-benzimidazole. Figure S12: GC spectrum (**a**) and MS data (**b**) of the as-synthesized 2-(2-methylphenyl)-1H-benzimidazole. Figure S13: GC spectrum (**a**) and MS data (**b**) of the as-synthesized 2-(3-methylphenyl)-1H-benzimidazole. Figure S14: GC spectrum (**a**) and MS data (**b**) of the as-synthesized 2-(4-methylphenyl)-1H-benzimidazole. Figure S15: GC spectrum (**a**) and MS data (**b**) of the as-synthesized 2-(3-methoxyphenyl)-1H-benzimidazole. Figure S16: GC spectrum (**a**) and MS data (**b**) of the as-synthesized 2-(4-methoxyphenyl)-1H-benzimidazole. Figure S17: GC spectrum (**a**) and MS data (**b**) of the as-synthesized 2-ethyl-1H-benzimidazole. Figure S18: GC spectrum (**a**) and MS data (**b**) of the as-synthesized 2-propyl-1H-benzimidazole.

Author Contributions

J.W.: Writing—original draft, Methodology, Investigation, Data curation. T.L.: Project administration, Investigation, Formal analysis. X.D.: Validation, Investigation. Z.L.: Writing—review & editing, Supervision, Conceptualization. All authors have read and agreed to the published version of the manuscript.

Funding

This research was funded by the NSFC (22372038, 22502081). Z.L. thanks the Award Program for Minjiang Scholar Professorship for financial support.

Institutional Review Board Statement

Not applicable.

Informed Consent Statement

Not applicable.

Data Availability Statement

Data will be made available on request.

Conflicts of Interest

The authors declare no conflict of interest.

Use of AI and AI-Assisted Technologies

No AI tools were utilized for this paper.

References

1. Zhang, N.; Gong, W.B.; Xiong, Y.J. Modern organic transformations: Heterogeneous thermocatalysis or photocatalysis? *Chem. Soc. Rev.* **2025**, *54*, 5189–5223.
2. Climent, M.J.; Corma, A.; Iborra, S. Heterogeneous catalysts for the one-pot synthesis of chemicals and fine chemicals. *Chem. Rev.* **2011**, *111*, 1072–1133.
3. Patra, S.; Maity, N. Recent advances in (hetero)dimetallic systems towards tandem catalysis. *Coord. Chem. Rev.* **2021**, *434*, 213803.
4. Hong, F.L.; Ye, L.W. Transition metal-catalyzed tandem reactions of ynamides for divergent N-heterocycle synthesis. *Acc. Chem. Res.* **2020**, *53*, 2003–2019.
5. Correia, J.T.M.; Santos, M.S.; Pissinati, E.F.; et al. Recent advances on photoinduced cascade strategies for the synthesis of N-heterocycles. *Chem. Rec.* **2021**, *21*, 2666–2687.
6. Rodenes, M.; Dhaeyere, F.; Martín, S.; et al. Multifunctional catalysis of nanosheet defective molybdenum sulfide basal planes for tandem reactions involving alcohols and molecular hydrogen. *ACS Sustain. Chem. Eng.* **2023**, *11*, 12265–12279.
7. Hao, M.M.; Li, Z.H. Visible light-initiated synergistic/cascade reactions over metal-organic frameworks. *Sol. RRL* **2021**, *5*, 2000454.
8. Chen, J.R.; Hu, X.Q.; Lu, L.Q.; et al. Exploration of visible-light photocatalysis in heterocycle synthesis and functionalization: Reaction design and beyond. *Acc. Chem. Res.* **2016**, *49*, 1911–1923.
9. Preston, P.N. Synthesis, reactions, and spectroscopic properties of benzimidazoles. *Chem. Rev.* **1974**, *74*, 279–314.
10. Lee, K.J.; Janda, K.D. Traceless solid-phase synthesis of 5-benzoylbenzimidazoles. *Can. J. Chem.* **2001**, *79*, 1556–1561.
11. Qin, Y.H.; Hao, M.M.; Ding, Z.X.; et al. Pt@MIL-101(Fe) for efficient visible light initiated coproduction of benzimidazoles and hydrogen from the reaction between *o*-phenylenediamines and alcohols. *J. Catal.* **2022**, *410*, 156–163.
12. Shiraishi, Y.; Sugano, Y.; Tanaka, S.; et al. One-pot synthesis of benzimidazoles by simultaneous photocatalytic and catalytic reactions on Pt@TiO_2 nanoparticles. *Angew. Chem. Int. Ed.* **2010**, *49*, 1656–1660.
13. Du, X.; Wang, J.Q.; Liu, H.R.Q.; et al. Visible-light-initiated dehydrogenative cyclization of *o*-aminobenzamide and alcohols for coproduction of quinazolinones and hydrogen over PtS/$ZnIn_2S_4$. *Sol. RRL* **2023**, *7*, 2300695.
14. Liu, H.R.Q.; Wu, S.Y.; Li, Z.H. Enabling an efficient light initiated one-pot synthesis of benzimidazoles over multifunctional 2D Pt/Ni-Fe-MOF nanosheets. *J. Catal.* **2025**, *447*, 116119.
15. Zhang, X.R.; Ye, H.L.; Liang, Y.J.; et al. Zinc indium sulfide-based photocatalysts for selective organic transformations. *Chemcatchem* **2024**, *16*, e202301553.
16. Hao, H.M.; Lang, X.J. Metal sulfide photocatalysis: Visible-light-induced organic transformations. *Chemcatchem* **2019**, *11*, 1378–1393.
17. Yu, Q.; Sun, S.H.; Puente-Santiago, A.R.; et al. Zinc mediated electronic structure of CoP toward photocatalytic H_2 evolution. *Appl. Catal. B-Environ.* **2025**, *367*, 125098.
18. Wang, J.Q.; Li, Y.X.; Liu, H.R.Q.; et al. Depolymerization of native lignin over thiol capped ultrathin $ZnIn_2S_4$ microbelts mediated by photogenerated thiyl radical. *Angew. Chem. Int. Ed.* **2024**, *63*, e202410397.
19. Kuang, P.Y.; Sayed, M.; Fan, J.J.; et al. 3D graphene-based H_2 production photocatalyst and electrocatalyst. *Adv. Energy Mater.* **2020**, *10*, 1903802.
20. Hummers, W.S.; Offeman, R.E. Preparation of graphitic oxide. *J. Am. Chem. Soc.* **1958**, *80*, 1339.
21. Wang, X.L.; Li, Y.Y.; Li, Z.H. Efficient visible light initiated hydrothiolations of alkenes/alkynes over Ir_2S_3/$ZnIn_2S_4$: Role of Ir_2S_3. *Chin. J. Catal.* **2021**, *42*, 409–416.
22. Wang, M.Y.; Wang, P.H.; Long, Y.; et al. Improved H-adsorption ability of Cu in CuNi alloy nanodots toward the efficient photocatalytic H_2-evolution activity of TiO_2. *Dalton Trans.* **2022**, *51*, 14526–14534.
23. Ding, G.Z.; Zhang, Y.G.; Chen, C.Y.; et al. Constructing a dual-functional 0D/2D-3D PtO/$ZnIn_2S_4$ photocatalyst for phenylcarbinol oxidation and H_2 production under visible light. *J. Alloys Compd.* **2025**, *1037*, 182338.
24. Liu, F.J.; Gao, Y.; Chi, X.H.; et al. A PtS QDs/$ZnIn_2S_4$ heterojunction catalyst for efficient photocatalytic hydrogen production and reduction of *p*-nitrophenol. *J. Environ. Chem. Eng.* **2022**, *10*, 108840.
25. Wang, J.H.; Li, H.; Cai, Y.H.; et al. Direct blue light-induced autocatalytic oxidation of *o*-phenylenediamine for highly sensitive visual detection of triaminotrinitrobenzene. *Anal. Chem.* **2019**, *91*, 6155–6161.
26. Sheng, Y.Q.; Miao, H.; Jing, J.F.; et al. Perylene diimide anchored graphene 3D structure via π-π interaction for enhanced photoelectrochemical degradation performances. *Appl. Catal. B-Environ.* **2020**, *272*, 118897.